[American Journal of Science, Vol. 309, June, 2009, P. 431–449, DOI 10.2475/06.2009.01]

American Journal of Science

JUNE 2009

EXSOLUTION BY SPINODAL DECOMPOSITION I: EVOLUTION EQUATION FOR BINARY MINERAL SOLUTIONS WITH ANISOTROPIC INTERFACIAL ENERGY

E. PETRISHCHEVA and R. ABART

Institute of Geological Sciences, Freie Universität Berlin, Malteserstrasse 74-100, D-12249, Berlin, Germany

ABSTRACT. Phase separation in a binary system that results from the uphill diffusion of chemical components is investigated theoretically. We reconsider the original spinodal decomposition model of Cahn and Hilliard taking into account possible intrinsic anisotropy of the underlying system. Specifically we address the effects of orientation dependent interfacial energy. Such anisotropy is of particular importance for mineral systems. The corresponding evolution equation is systematically derived. We show how the anisotropy affects the interfacial energy per unit area, the interface width, scaling laws, and the critical system size at which spinodal decomposition starts to develop. We further obtain numerical solutions and discuss coarsening dynamics for the case where the decomposition products have pronounced shape anisotropy.

INTRODUCTION

Many rock forming minerals pertain to solid solution series. If a solution phase, which is chemically homogeneous at high temperatures, is brought into a polyphase equilibrium domain, for instance, by cooling, it may unmix. Phase separation may either occur by nucleation and growth or by spinodal decomposition. The latter is the kinetic pathway for exsolution, if the originally homogeneous phase is at a condition, where it is unstable with respect to small compositional fluctuations. Spinodal decomposition occurs by inter diffusion of the chemical constituents. There is no nucleation barrier that needs to be overcome and compositional fluctuations grow spontaneously. Spinodal decomposition is believed to be rapid compared to exsolution by nucleation and growth, and it is hence expected to be important in rapidly cooled rocks and in cases where nucleation kinetics is sluggish. Exsolution by spinodal decomposition has indeed been reported repeatedly from minerals that were cooled rapidly. Among others, spinodal decomposition has been described from alkali feldspar (Brown and Parsons, 1984; Smith and Brown, 1988), pyroxene (Weinbruch and Muller, 1995) and spinel (Price, 1982). Spinodal decomposition has also been produced experimentally for rock forming minerals (Yund and others, 1974; McCallister and Yund, 1977; Yund and Davidson, 1978; Grove, 1982; Hovis and others, 2003; Weinbruch and others, 2003; Golla-Schindler and others, 2005).

Spinodal decomposition starts with the formation of periodic modulations of the composition within the initially homogeneous solution phase. The amplitude and the characteristic wavelength (dimension) of these modulations depend on reaction affinity, that is on the degree of supersaturation of the originally homogeneous solution phase with respect to the decomposition products. In addition the characteristic wavelength depends on the contribution of the newly formed phase boundaries to the system free energy; that is on the free energy density of the newly formed phase

boundaries. The compositional modulations grow until equilibrium compositions are attained in the decomposition products. This evolution is referred to as the phase separation stage. The phase separation stage is followed by coarsening of the exsolution microstructure. Coarsening is primarily diffusion controlled (McCallister and Yund, 1977; Ratke and Voorhees, 2002; Weinbruch and others, 2003) and, hence, time and temperature dependent. Microstructures developed from spinodal decomposition and subsequent coarsening thus have potential as geo-speedometers (Yund and Chapple, 1980; Price, 1982; Brizi and Mellini, 1982; Grove, 1982; Brown and Parsons, 1984, 1988; Watanabe and others, 1985; Smith and Brown, 1988; Weinbruch and Muller, 1995; Weinbruch and others, 2001). Experimental calibrations of potential exsolution speedometers have been provided for feldspar (Yund and others, 1974; Yund and Davidson, 1978; Hovis and others, 2003) and for pyroxene (McCallister and Yund, 1977; Grove, 1982; Weinbruch and others, 2001, 2003). These studies focus on the kinetics of coarsening and generally find that the characteristic dimension of exsolution microstructures scales with the third root of time during isothermal annealing experiments. All these studies only make use of the characteristic dimensions of exsolution microstructures and integrate the contributions of phase boundary energy and chemical diffusion into a single rate constant. They do not, however, exploit the information that is stored in the compositions of the decomposition products, in chemical zoning patterns, and in the microstructures that develop during phase separation and subsequent coarsening. Application of novel techniques in micro machining with focused ion beam and in analytical electron microscopy (Cheng and others, 1998; Kral and others, 2000) allows to determine phase compositions, chemical zoning patterns, precipitate morphologies and microstructures even in fine grained exsolution microstructures, where characteristic dimensions are in the sub micrometer range. A wealth of information can thus be extracted from exsolution microstructures, which may serve to calibrate advanced kinetic models.

This motivates us to develop a more general formulation of spinodal decomposition that reflects the underlying physics of phase separation. We choose a macroscopic approach (see, for instance, Heermann, 1984; Cahn and Novick-Cohen, 1994) for the microscopic treatment of spinodal decomposition) and revisit the formalism originally introduced by Cahn and Hilliard (Cahn and Hilliard, 1953; Chan, 1968). We adopt this model for the description of spinodal decomposition in an anisotropic binary system. The anisotropy can be introduced in several ways. First, elastic terms in the free energy density are anisotropic and predictably depend on direction (see Fischer and others, 1994; Taylor and Cahn, 1998; Abinandanan and Haider, 2001; Wise and others, 2007). Next, systems with symmetry less than cubic may have diffusion anisotropy, which may result in quasi-onedimensional patterns (Kuhl and Schmid, 2006). In this contribution we investigate a different anisotropy mechanism, namely, we allow for anisotropy of the interfacial energy. This mechanism is of particular importance for mineral systems and in this respect is poorly investigated in the current literature. In part I of this communication we review the basic thermodynamic concepts and the dynamical model for phase separation that is based on Cahn-Hilliard theory. We then introduce a generalization of the Cahn-Hilliard model that allows for intrinsic anisotropy of interfacial energy following the strategy first outlined in Cahn and Hilliard (1958). In the light of this generalization, we investigate how the anisotropy affects the interfacial energy per unit area, the interface width, scaling laws, and the critical system size at which spinodal decomposition starts to develop. Then we illustrate our findings using numerical solutions of the anisotropic model. The continuum mechanical aspects of corresponding phase transformations (for instance, induced stresses and their feedback effect on the phase separation) are ignored here. In part II of this communication we apply this theory to model exsolution of hypersolvus alklai feldspar during slow

cooling. In particular we address the potential of characteristic lamellar width and compositions as geo-speedometers. Even if idealizations must be made and certain details of the sub-solidus phase relations of the alkali feldspars cannot be captured, the modeling presented in part II provides new insights into the interplay of microstructural and chemical evolution of perthites during slow cooling.

EQUILIBRIUM SYSTEM

A macroscopic equilibrium system in which several phases coexist stably is usually described with a sharp boundaries approximation. The system is divided by a network of sharp boundaries into several uniform subsystems, where usual thermodynamic equations apply. Alternative theories like that originally developed by Cahn and Hilliard (Cahn and Hilliard, 1958) account for the inner structure of the transition regions between the phases assuming that they have a diffuse nature. In addition to the total number of atoms N_α for each component $\alpha = A, B, C \ldots$ also the spatial distribution of atoms becomes important here. The theory necessarily operates with the local number of atoms per unit volume $n_\alpha(\mathbf{r})$. The latter is a smooth function of the space variable $\mathbf{r}$ for each α. Thermodynamic potentials such as Gibbs free energy $\mathcal{G}$ can additionally depend on the spatial derivatives $\nabla n_\alpha(\mathbf{r})$ and are considered as functionals, that is,

$$\mathcal{G} = \int G(P, T, n, \nabla n) d^3\mathbf{r}, \tag{1}$$

where G is the Gibbs free energy per unit volume, the integration is performed over the volume domain occupied by the system, n is a short notation for all atomic densities, P and T being the local pressure and temperature. In what follows we will consider a system with a constant temperature under a constant and isostatic external load. To determine chemical potentials and thereafter equilibrium conditions one considers a redistribution of atoms resulting in a variation of the atomic densities $n_\alpha \to n_\alpha + \delta n_\alpha$. Using the divergence theorem and assuming that the system boundaries do not contribute to $\delta\mathcal{G}$, the corresponding variation of the free energy (1) can be presented as

$$\delta\mathcal{G} = \int \left(\sum_\alpha \mu_\alpha \delta n_\alpha \right) d^3\mathbf{r}, \tag{2}$$

where generalized chemical potentials μ_α are defined as variational derivatives:

$$\mu_\alpha = \frac{\delta\mathcal{G}}{\delta n_\alpha} = \frac{\partial G}{\partial n_\alpha} - \nabla \cdot \frac{\partial G}{\partial(\nabla n_\alpha)}. \tag{3}$$

In general, a fluctuation δn_α will change both the local stresses and the total volume occupied by the system. For the sake of simplicity we only consider a special case of interdiffusion which occurs by "exchange" of atoms in a sublattice where the remainder of the crystal structure remains unchanged such that macroscopic displacements and mechanical stresses are not induced. The specific flux model that accounts for the interdiffusion will be specified in the next section.

The equilibrium state of an isothermal-isobaric system is determined by conditional minimization of the free energy under the restriction that the total number of atoms for each component conserves

$$\min_{n(\mathbf{r})} \mathcal{G} \quad \text{such that} \quad N_\alpha = \int n_\alpha(\mathbf{r})\, d^3\mathbf{r} = \text{const.}$$

In accord with Lagrange's method instead of $\mathcal{G}$ a modified free energy is minimized

$$\mathcal{G}_L = \mathcal{G} - \sum_{\alpha} \mu_{\alpha 0} \int n_\alpha(\mathbf{r})\, d^3\mathbf{r}, \tag{4}$$

where the constant factors $\mu_{\alpha 0}$ are yet unknown Lagrange multipliers. Minimization of $\mathcal{G}_L$ requires solution of the corresponding Euler-Lagrange equations

$$0 = \frac{\delta \mathcal{G}_L}{\delta n_\alpha} = \frac{\delta \mathcal{G}}{\delta n_\alpha} - \mu_{\alpha 0} = \mu_\alpha - \mu_{\alpha 0}. \tag{5}$$

In other words, the Lagrange multiplier $\mu_{\alpha 0}$ is the equilibrium value of the generalized chemical potential μ_α introduced in equation (3).

As a specific example we consider a binary system with $\alpha = A, B$ and

$$G(n) = (n_A + n_B) g(a), \tag{6}$$

where $a = n_A/(n_A + n_B)$ and $g(a)$ is a mean free energy per atom. The quantity in (4) that has to be minimized reads

$$\mathcal{G}_L = \int (n_A + n_B) \Delta g(a) d^3\mathbf{r},$$

where following (Chan and Hilliard, 1958) we use a notation

$$\Delta g(a) = g(a) - a\mu_{A0} - (1 - a)\mu_{B0}. \tag{7}$$

The chemical potentials of components are directly derived from the definition (3)

$$\mu_A = g(a) + (1 - a)\frac{\partial g}{\partial a}, \tag{8}$$

$$\mu_B = g(a) - a\frac{\partial g}{\partial a}. \tag{9}$$

Using the latter expressions we reduce the equilibrium conditions (eq. 5) to the form

$$g(a) = a\mu_{A0} + (1 - a)\mu_{B0}, \tag{10}$$

$$\frac{\partial g}{\partial a} = \mu_{A0} - \mu_{B0} \tag{11}$$

or

$$\Delta g(a) = 0 \quad \text{and} \quad \frac{\partial}{\partial a}\Delta g(a) = 0.$$

Equations (10)–(11) have a simple geometrical interpretation. Any uniform concentration $a = a_0$ is a valid equilibrium state if the straight line $a\mu_{A0} + (1 - a)\mu_{B0}$ on the $a - g$ plane is tangent to the free energy density curve $g(a)$ at $a = a_0$. Thereby both μ_{A0} and μ_{B0} are uniquely defined. If $g''(a_0) = \Delta g''(a_0) > 0$ the modified free energy takes its minimum at $a = a_0$ and the equilibrium is stable. Unstable uniform solutions are possible for a concave-convex $g(a)$ curve (see fig. 1). The region of the unstable concentrations is determined by the spinodal (inflection) points a_{s1}, a_{s2} such that

$$g''(a_{s1}) = g''(a_{s2}) = 0$$

$$g''(a) < 0 \quad \text{for} \quad a_{s1} < a < a_{s2}$$

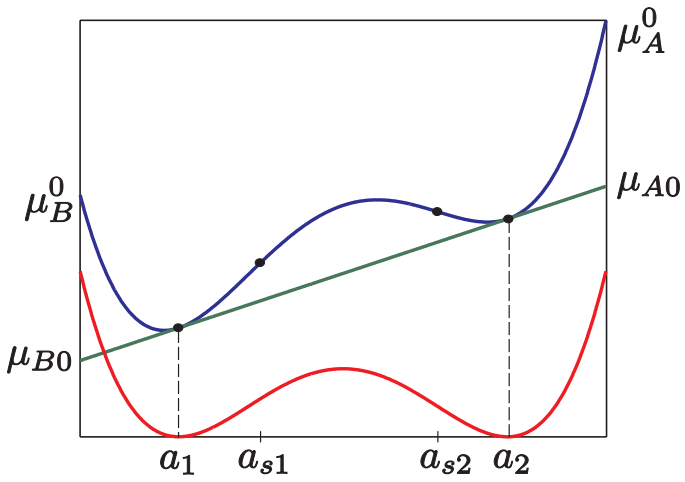

Fig. 1. Graphical representation of $g(a)$ (blue curve), $a\mu_{A0} + (1 - a)\mu_{B0}$ (green line), and $\Delta g(a)$ (red curve) in a binary system that allows for phase separation. The spinodal points $a_{s1,s2}$ are inflection points such that $g''(a) = 0$. For any initial value of a between the spinodal points the system decomposes spontaneously into two phases with their compositions defined by the binodal points $a_{1,2}$ such that $g'(a) = \mu_{A0} - \mu_{B0}$ and $g''(a) > 0$. The parameters μ_{A0} and μ_{B0} are the equilibrium chemical potentials of components.

In the presence of inflection points in the $g(a)$ curve a stable coexistence of two phases with the concentrations a_1 and a_2 (binodal points) is possible as determined by the common tangent (shown in fig. 1). Both $a = a_1$ and $a = a_2$ are valid solutions of the system (eq. 10)–(eq. 11). In what follows we will always assume that $a_1 < a_{s1} < a_{s2} < a_2$.

DYNAMICAL MODEL

To describe the dynamics of phase separation a suitable evolutionary equation is derived based on a continuity equation for the atomic density n_α

$$\partial_t n_\alpha = -\nabla \cdot \mathbf{j}_\alpha \tag{12}$$

which is supplemented by a general Onsager model for the atomic flux (Onsager, 1931)

$$\mathbf{j}_\alpha = \sum_\beta L_{\alpha\beta} \nabla \mu_\beta \tag{13}$$

for constant P and T. Here the mobility matrix is symmetric $L_{\alpha\beta} = L_{\beta\alpha}$ and we impose an additional restriction

$$\sum_\alpha L_{\alpha\beta} = 0 \tag{14}$$

such that the total flux automatically vanishes

$$\sum_\alpha \mathbf{j}_\alpha = \sum_{\alpha,\beta} L_{\alpha\beta} \nabla \mu_\beta = \sum_\beta \nabla \mu_\beta \sum_\alpha L_{\alpha\beta} = 0.$$

Therefore the total number of atoms per unit volume $\mathfrak{n}$ remains constant

$$\mathfrak{n} = \sum_\alpha n_\alpha(\mathbf{r}, t) = \text{const.} \tag{15}$$

in accord with the interdiffusion condition. An important macroscopic consequence of the dynamical model (eq. 13)–(eq. 14) is that the system evolution with constant P and T leads to a permanent decrease of the free energy $\mathcal{G}(t)$. This fact provides a direct link to the thermodynamic considerations from the previous section. In accord with the definition (eq. 2) of chemical potential we obtain

$$\frac{d\mathcal{G}}{dt} = \int \left(\sum_{\alpha} \mu_{\alpha} \partial_t n_{\alpha} \right) d^3\mathbf{r} = \sum_{\alpha} \int \mathbf{j}_{\alpha} \cdot \nabla \mu_{\alpha} d^3\mathbf{r}$$

where we used equation (12) to eliminate $\partial_t n_{\alpha}$ and performed partial integration. Note, that at the boundary the normal component of $\mathbf{j}_{\alpha}$ is zero because the system is closed. For the flux model (eq. 13) we obtain

$$\frac{d\mathcal{G}}{dt} = \sum_{\alpha,\beta} \int L_{\alpha\beta} \nabla \mu_{\alpha} \nabla \mu_{\beta} d^3\mathbf{r}.$$

Using equation (14) we transform the latter expression to the form

$$\frac{d\mathcal{G}}{dt} = -\frac{1}{2} \sum_{\alpha,\beta} \int L_{\alpha\beta} (\nabla \mu_{\alpha} - \nabla \mu_{\beta})^2 d^3\mathbf{r}$$

so that indeed $d\mathcal{G}/dt \leq 0$.

For a binary system with $\alpha = A, B$ the mobility matrix $L_{\alpha\beta}$ takes an especially simple form

$$L_{\alpha\beta} = \begin{pmatrix} -L & L \\ L & -L \end{pmatrix}$$

in which only one mobility $L = L_{AB}$ counts. The fluxes are given by the expression

$$\mathbf{j}_A = -\mathbf{j}_B = -L_{AB} \nabla (\mu_A - \mu_B). \tag{16}$$

According to (Nauman and He, 2001) the mobility L_{AB} must be concentration dependent and vanish if either $n_A = 0$ or $n_B = 0$. It is then useful to introduce a coefficient D such that

$$L_{AB} = \frac{D}{kT} \frac{n_A n_B}{\mathfrak{n}}, \tag{17}$$

where kT is temperature in energetic units and coefficient D will be identified as a diffusion constant. The latter is assumed to be identical for both components. Note, that in contrast with the natural binary diffusion in alloys such an assumption can be violated in crystalline solids in which both self-diffusion and interdiffusion occurs by the vacancy mechanism (Shewmon, 1963). In the present simple model a direct exchange of a and b with no change in vacancy concentration is assumed. Consequently the diffusivity parameter D becomes the same for both components.

For the free energy (eq. 6) equations (8) and (9) yield $\mu_A - \mu_B = \partial g / \partial a$. Applying equations (16) and (17) we obtain

$$\mathbf{j}_A = -\mathbf{j}_B = -\frac{D}{kT} \mathfrak{n} a (1 - a) \frac{\partial^2 g}{\partial a^2} \nabla a. \tag{18}$$

Furthermore, $\nabla a = (1/\mathfrak{n}) \nabla n_A$ due to equation (15) and therefore $\mathbf{j}_A = -D_{\text{eff}}(a) \nabla n_A$, where

$$D_{eff}(a) = D\frac{a(1-a)}{kT}\frac{\partial^2 g}{\partial a^2} \tag{19}$$

is naturally interpreted as a nonlinear diffusion coefficient. In the previous section we have shown that the uniform distribution of atoms is unstable if $g''(a) < 0$. Now we can conclude that the instability in question corresponds to the uphill diffusion of the components. The system is governed by a single nonlinear diffusion equation (Nauman and He, 2001)

$$\partial_t a = \nabla \cdot [D_{eff}(a)\nabla a], \tag{20}$$

which is obtained from equations (12) and (18). For instance, let us consider the following expression for the free energy per atom of a regular solution

$$g(a) = \mu_A^0 a + \mu_B^0 b + kT(a \ln a + b \ln b) + Wab, \tag{21}$$

where $W > 0$ is the interaction parameter, $b = 1 - a$, and μ_A^0 and μ_B^0 are the chemical potentials of the pure phase components. The last two terms in equation (21) account for the configurational and for the non-ideality contributions to the free energy, in general $W = W(P, T)$. A direct calculation in accord with equation (19) results in

$$D_{\text{eff}}(a) = D\left[1 - 2a(1-a)\frac{W}{kT}\right]$$

so that classical diffusion takes place if $W = 0$ and the spinodal points first appear if

$$W \geq 2kT, \tag{22}$$

the latter inequality determines the decomposition threshold. Clearly $a_0 = \frac{1}{2}$ is the most unstable value among the possible uniform concentrations. The free energy of mixing is shown in figure 2 against a for several values of $W/(kT)$. Also the binodal and spinodal concentrations are shown in $W/(kT) - a$ space.

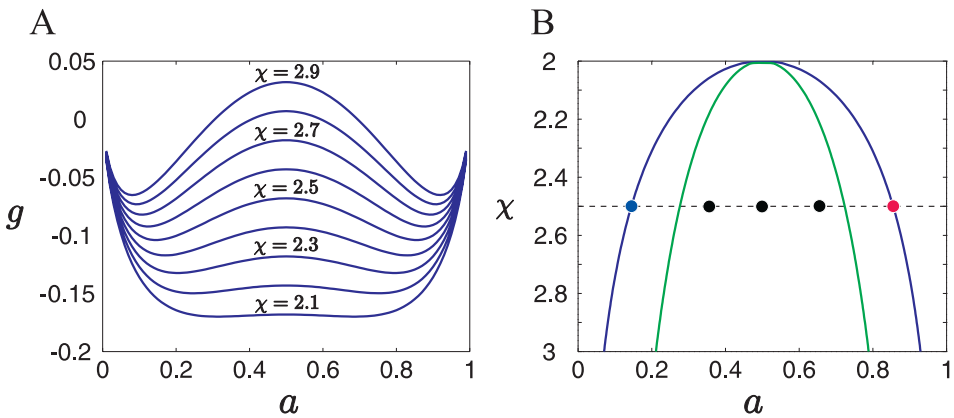

Fig. 2. (A) Free energy of a regular solution, as given by the two last terms in equation (21), versus concentration a for different values of $\chi = W/(kT) > 2$. (B) solvus diagram on $a - \chi$ plane. Blue line: solvus, that is, relation between W and $a_{1,2}$. Green line: spinode, that is, relation between W and $a_{s1,s2}$. The three black dots correspond to the initial uniform concentrations for the three numerical examples presented in figure 3. In all cases, blue and red dots correspond to the equilibrium concentrations of the decomposing phases.

CAHN-HILLIARD THEORY

Equation (20) correctly predicts the instability region, however, mathematically the corresponding problem is poorly posed, that is, the final solution randomly jumps between the phases in the neighboring points of the numerical grid and therefore depends on discretization (Nauman and He, 2001). Following (Cahn and Hilliard, 1958), regularization is gained by taking into account phase boundaries, that is, transition regions with $\nabla a \neq 0$, which contribute to the system free energy. To this end one introduces a generalization of the free energy density (eq. 6) by replacing $G(n) = (n_A + n_B)g(a)$ with

$$G(n, \nabla n) = (n_A + n_B)\mathfrak{g}(a, \nabla a, \nabla(\nabla a), \ldots),$$

where $\nabla(\nabla a)$ abbreviates nine second order derivatives $\partial_i\partial_j a$ with the indices $i, j = 1, 2, 3$. We assume that the system is invariant under the mirror $\mathbf{r} \rightarrow -\mathbf{r}$ transformation so that the free energy density cannot depend on $\partial_i a$ directly, whereas the dependence on $(\partial_i a)^2$ or on $\partial_i\partial_j a$ is possible. Further, if l is a characteristic length scale associated with the interface we assume that

$$l\nabla a \sim \epsilon a, \quad l^2\nabla(\nabla a) \sim \epsilon^2 a, \quad \textit{et cetra},$$

where $\epsilon \ll 1$ so that the contribution of the high-order terms in $\mathfrak{g}$ is smaller than that of the low-order terms. Note, that $\nabla a \approx (a_2 - a_1)/l$ in the transition region, so that strictly speaking the theory can be applied only if $a_2 - a_1 \ll 1$, that is, near the decomposition threshold (eq. 22). Qualitatively reasonable results can, however, be expected also for $a_1 - a_2 \sim 1$. Using Taylor expansion of $\mathfrak{g}$ and accounting only for the leading terms one obtains

$$\mathfrak{g}(a, \nabla a, \nabla(\nabla a)) = g(a) + A_{ij}(a)\partial_i a\partial_j a + B_{ij}(a)\partial_i\partial_j a,$$

where $A_{ij}(a)$ and $B_{ij}(a)$ are related to the derivatives of $\mathfrak{g}$ and summation over the dummy indices is assumed. Following the strategy of Cahn and Hilliard (1958) one can reduce the expansion for $\mathfrak{g}$ to

$$\mathfrak{g}(a, \nabla a) = g(a) + \frac{1}{2}\kappa_{ij}(a)\partial_i a\partial_j a, \tag{23}$$

where the second-order tensor $\kappa_{ij}(a)$ is expressed in terms of $A_{ij}(a)$ and $B_{ij}(a)$

$$\frac{1}{2}\kappa_{ij}(a) = A_{ij}(a) - \frac{d}{da}B_{ij}(a).$$

The artificial factor ½ was introduced in equation (23) to avoid an unnecessary factor in the final equation. As any compositional heterogeneity contributes positively to the system free energy, the expression $\kappa_{ij}\partial_i a\partial_j a$ must be positive for any direction of ∇a. The tensor κ_{ij} is therefore positively defined. The dependence of κ_{ij} on a can be actually ignored, because $a_1 \approx a_2$. The generalized expression for the free energy (eq. 23) is now substituted into the definition (eq. 3)

$$\mu_\alpha = \frac{\delta}{\delta n_\alpha}\int (n_A + n_B)\left[g(a) + \frac{1}{2}\kappa_{ij}\partial_i a\partial_j a\right]d^3\mathbf{r}$$

for $\alpha = A, B$. After calculation of the variational derivatives we find that the chemical potentials (eq. 8) and (eq. 9) become

$$\mu_A = \mathfrak{g}(a, \nabla a) + (1 - a)\left(\frac{\partial g}{\partial a} - \kappa_{ij}\partial_i\partial_j a\right), \tag{24}$$

$$\mu_B = \mathfrak{g}(a, \nabla a) - a\left(\frac{\partial g}{\partial a} - \kappa_{ij}\partial_i\partial_j a\right) \tag{25}$$

so that

$$\mu_A - \mu_B = \frac{\partial g}{\partial a} - \kappa_{ij}\partial_i\partial_j a. \tag{26}$$

Finally, using the flux model (eq. 16) and continuity equation (12) we arrive to the equation

$$\partial_t a = \frac{D}{kT}\nabla \cdot \left[a(1 - a)\nabla\left(\frac{\partial g}{\partial a} - \kappa_{ij}\partial_i\partial_j a\right)\right], \tag{27}$$

which is a natural generalization of the nonlinear diffusion equation (20). Equation (27) is the basic equation for our further consideration of spinodal decomposition. The presented derivation is a systematic generalization of the original Cahn-Hilliard approach. The tensor κ_{ij} contains information on possible anisotropy of the medium, either internal or caused by an externally imposed stress. It can be transformed to its main axes

$$\kappa_{ij}\partial_i\partial_j a \rightarrow \kappa_1\partial_x^2 a + \kappa_2\partial_y^2 a + \kappa_3\partial_z^2 a$$

into a single space domain by a proper rotation. Equation (27) reduces to the classical Cahn-Hilliard equation in an isotropic medium with $\kappa_{ij} = \kappa\delta_{ij}$ where δ_{ij} is Kronecker delta

$$\partial_t a = \frac{D}{kT}\nabla \cdot \left[a(1 - a)\nabla\left(\frac{\partial g}{\partial a} - \kappa\nabla^2 a\right)\right].$$

As a specific example, the anisotropic model (eq. 27) will be used together with equation (21) for the free energy of a regular solution. In this case the final equation reads

$$\partial_t a = D\nabla \cdot \left\{\left[1 - 2a(1 - a)\frac{W}{kT}\right]\nabla a - a(1 - a)\frac{\nabla\kappa_{ij}\partial_i\partial_j a}{kT}\right\}. \tag{28}$$

In what follows, we will investigate an anisotropy effect on phase decomposition using the model equations derived above. When possible, the results will be given in a general form with equation (27). Equation (28) will be used as a specific example, which will be also compared to the classical Cahn-Hilliard model.

STABILITY ANALYSIS AND CRITICAL SYSTEM SIZE

In this section we discuss stability of a uniform equilibrium state $a = a_0$. Here, one must distinguish between stability with respect to *infinitesimal* and stability with respect to *finite* perturbations. When the system in question is in a metastable region of the parameter space, it can be destabilized by a large fluctuation by which an inclusion of the second (thermodynamically favorable) phase is created. Concerning spinodal decomposition, we are interested in a system that is destabilized by a small perturbation characterized by a wave vector $\boldsymbol{K}$. When the system is isotropic, the region of unstable wave vectors is determined by the inequality (Nauman and He, 2001)

$$\boldsymbol{K}^2 < -\frac{g_0''}{\kappa}, \tag{29}$$

where $g_0'' = (\partial^2 g/\partial a^2)_{a=a_0}$. If the system in question is small enough the instability is suppressed simply because perturbations with unstable wavelengths are incompatible

with the boundary conditions. Consider, for instance, a cubic system with $0 < x, y, z < L$ and no flux boundary conditions. The smallest possible wave vector of a compatible perturbation is π/L, phase separation occurs if the condition (29) is satisfied. Therefore the instability is suppressed if

$$L \leq \pi \sqrt{\frac{\kappa}{-g_0''}}. \tag{30}$$

We now generalize equations (29) and (30) for an anisotropic system. Consider a small perturbation $\tilde{a}$ of the otherwise uniform equilibrium state $a = a_0$

$$a(\mathbf{r}, t) = a_0 + \tilde{a}(\mathbf{r}, t), \quad a_0 = \text{const}, \quad \tilde{a} \ll 1.$$

Equation (27) is linearized to the form

$$\partial_t \tilde{a} = a_0(1 - a_0) \frac{D}{kT} \nabla^2 (g_0'' \tilde{a} - \kappa_{ij} \partial_i \partial_j \tilde{a}).$$

Given a periodic perturbation in the form of a Fourier harmonic $\tilde{a}(\mathbf{r}, t) \sim \exp(i\boldsymbol{K} \cdot \mathbf{r})$, we obtain

$$\partial_t \tilde{a} = a_0(1 - a_0) \frac{DK^2}{kT} (-g_0'' - \kappa_{ij} K_i K_j) \tilde{a}.$$

The harmonic in question is stable if $\partial_t \tilde{a}/\tilde{a} < 0$ and unstable otherwise. The term $\kappa_{ij} K_i K_j \geq 0$ always tends to stabilize the system and always dominates for small wavelengths. If $g_0'' > 0$ the system is stable irrespective of the interfacial energy term. If $g_0'' < 0$ there is a region of unstable wave vectors determined by the inequality

$$\kappa_{ij} K_i K_j < -g_0''. \tag{31}$$

Equation (31) generalizes equation (29).

In an infinite system the spectrum of possible wave vectors is continuous and inequality (31) always can be satisfied. For a finite system the spectrum is discrete and the instability may be suppressed. For instance, consider a system in the form of a slab of width L_τ that is orthogonal to a unit vector $\boldsymbol{\tau}$. The instability always develops for $\boldsymbol{K} \perp \boldsymbol{\tau}$ but can still be suppressed for $\boldsymbol{K} \parallel \boldsymbol{\tau}$. The minimal wave vector for a corresponding perturbation is π/L_τ and the instability is suppressed if

$$L_\tau \leq \pi \sqrt{\frac{\kappa_{ij} \tau_i \tau_j}{-g_0''}}. \tag{32}$$

The latter condition generalizes equation (30). If the system is subject to periodic boundary conditions the factor π must be replaced by 2π. The effect of system size on pattern formation is further investigated in the section titled DYNAMICS OF PHASE SEPARATION.

EQUILIBRIUM STATES

In this section we discuss equilibrium solutions of equation (27), that is, solutions of the stationary equation

$$\nabla \cdot \left[a(1 - a) \nabla \left(\frac{\partial g}{\partial a} - \kappa_{ij} \partial_i \partial_j a \right) \right] = 0 \tag{33}$$

Here, an important advantage over the gradient-free models is that in addition to the uniform $a = \text{const}$ equilibrium states also nonuniform stationary solutions of equation (33) with $a = a(\mathbf{r})$ are possible. Furthermore, one can evaluate macroscopic system

parameters such as interfacial energy or width of the transition region and reveal their dependence on temperature.

Multiplying equation (33) with $\partial g/\partial a - \kappa_{ij}\partial_i\partial_j a$ and integrating over the system volume, one can obtain an integral relation

$$\int a(1-a)\left[\nabla\left(\frac{\partial g}{\partial a} - \kappa_{ij}\partial_i\partial_j a\right)\right]^2 d^3\mathbf{r} = 0, \tag{34}$$

where the divergence theorem and the no flux boundary condition were used. The integral relation (eq. 34) can be satisfied only if the expression

$$\frac{\partial g}{\partial a} - \kappa_{ij}\partial_i\partial_j a = \text{const.} \tag{35}$$

Far from the transition region the term $\kappa_{ij}\partial_i\partial_j a$ can be neglected such that equation (35) is a natural generalization of equation (11). In the section titled EQUILIBRIUM SYSTEM the concentrations $a = a_{1,2}$ of a two-phase equilibrium system state with $\mu_A = \mu_{A0}$ and $\mu_B = \mu_{B0}$ were found from the algebraic system (eq. 10)–(eq. 11). The latter is replaced with an ordinary differential equation in the Cahn-Hilliard theory

$$\frac{\partial g}{\partial a} - \kappa_{ij}\partial_i\partial_j a = \mu_{A0} - \mu_{B0}. \tag{36}$$

We consider $g(a)$ which has two local minima (fig. 1) and investigate the most simple case of a plane interface. Let $\boldsymbol{\tau}$ be a unit vector orthogonal to the interface. It is natural to assume that

$$a = a(\xi) \quad \text{with} \quad \xi = \boldsymbol{\tau}\cdot\mathbf{r}$$

so that actually the solution depends only on one local coordinate ξ which is orthogonal to the interface. The equilibrium equation (36) can be rewritten

$$\kappa_{ij}\tau_i\tau_j\frac{d^2a}{d\xi^2} - \frac{\partial}{\partial a}[g(a) - a\mu_{A0} - (1-a)\mu_{B0}] = 0 \tag{37}$$

such that $\Delta g(a)$ introduced in (eq. 7) is recognized. Equation (37) is multiplied with $da/d\xi$ and integrated to yield

$$\frac{\kappa_{ij}\tau_i\tau_j}{2}(\partial_\xi a)^2 = \Delta g(a) + \text{const.} \tag{38}$$

The latter equation can be solved for any $\Delta g(a)$ by separation of variables. Consider a special solution $a(\xi)$ corresponding to an interface between two equilibrium states $a = a_1$ and $a = a_2$ shown in figure 1. Here $\Delta g(a_1) = \Delta g(a_2) = 0$ (see fig. 1) and the integration constant in equation (38) vanishes. We immediately obtain that

$$\partial_\xi a = \sqrt{\frac{2\Delta g(a)}{\kappa_{ij}\tau_i\tau_j}}. \tag{39}$$

The corresponding solution $a = a(\xi)$ describes the final system state after decomposition. Such a solution is stable (Shinozaki and Oono, 1993; Bettinson and Rowlands, 1996).

Equation (39) can be used to relate the phenomenological parameters κ_{ij} and the interfacial energy γ_τ per unit area of the interface orthogonal to the vector $\boldsymbol{\tau}$. To this end we follow (Cahn and Hilliard, 1958) and calculate an interfacial part of the system free energy

$$\mathcal{G}_{\text{int}}=\int (n_A + n_B)\left[\Delta g + \frac{1}{2}\kappa_{ij}\partial_i a\partial_j a\right]d^3\mathbf{r}$$

for the above defined one-dimensional atomic distribution. The interfacial free energy per atom is given by the expression $\Delta g + \frac{1}{2}\kappa_{ij}\partial_i a\partial_j a$, which in accord to equation (38) is equal to $\kappa_{ij}\tau_i\tau_j(\partial_\xi a)^2$ for the solution in question. Therefore

$$\mathcal{G}_{\text{int}}=\mathfrak{n}A\kappa_{ij}\tau_i\tau_j\int_{-\infty}^{\infty}(\partial_\xi a)^2 d\xi = \mathfrak{n}A\kappa_{ij}\tau_i\tau_j\int_{a_1}^{a_2}\partial_\xi a\, da, \tag{40}$$

where the solution (39) is homogeneous in a plane orthogonal to $\boldsymbol{\tau}$ and therefore $d^3\mathbf{r}$ can be replaced with $Ad\xi$, where A is the area of the interface. By definition $\gamma_\tau = \mathcal{G}_{\text{int}}/A$ and substituting (39) into (40) we conclude that

$$\gamma_\tau = \mathfrak{n}\sqrt{2\kappa_{ij}\tau_i\tau_j}\int_{a_1}^{a_2}\sqrt{\Delta g(a)}\; da.$$

The latter equation explicitly reveals the dependence of the interfacial energy on orientation.

To give an example, we assume that the function $g(a)$ can be approximated by a fourth order polynomial. The deduced fourth order polynomial $\Delta g(a)$ both is equal to zero and has local minima at $a = a_1$ and $a = a_2$ (fig. 1). Therefore one may write

$$\Delta g(a) = \Lambda(a - a_1)^2(a - a_2)^2$$

for a properly chosen positive parameter Λ. Equation (39) reduces to

$$\partial_\xi a = \sqrt{\frac{2\Lambda}{\kappa_{ij}\tau_i\tau_j}}(a_2 - a)(a - a_1).$$

After a direct integration we get

$$\frac{a - a_1}{a_2 - a} = \exp\left[\sqrt{\frac{2\Lambda}{\kappa_{ij}\tau_i\tau_j}}(a_2 - a_1)\xi\right],$$

where we assumed that the interface is located at $\xi = 0$. Therefore the solution of equation (39) is

$$a(\xi) = \frac{a_1 + a_2 e^{\xi/l_\tau}}{1 + e^{\xi/l_\tau}},$$

where

$$l_\tau = \frac{1}{a_2 - a_1}\sqrt{\frac{\kappa_{ij}\tau_i\tau_j}{2\Lambda}} \tag{41}$$

is a characteristic width of the transition region. For the isotropic case the corresponding solution was originally found in (Cahn and Hilliard, 1958). In the anisotropic case the interfacial energy per unit area

$$\gamma_\tau = \mathfrak{n}\sqrt{\frac{\Lambda\kappa_{ij}\tau_i\tau_j}{2}}\frac{(a_2 - a_1)^3}{3} \tag{42}$$

depends on the orientation of the interface.

As a specific example we consider a mixing model (eq. 21) of regular solution assuming that

$$\frac{W}{kT} = 2 + \varepsilon \quad \text{with} \quad \varepsilon \ll 1$$

so that the system is slightly above the decomposition threshold and $a_{1,2} \approx 1/2$. Using Taylor expansion of the free energy of a regular solution (eq. 21) at $a = \frac{1}{2}$ where

$$a \ln a + (1 - a) \ln(1 - a) + (2 + \varepsilon)\, a(1 - a) = \frac{1}{2} - \ln 2 + \frac{\varepsilon}{4} - \varepsilon\left(a - \frac{1}{2}\right)^2 + \frac{4}{3}\left(a - \frac{1}{2}\right)^4 + \cdots$$

it is easy to verify that

$$\Delta g(a) = \frac{4}{3}\, kT\left[\left(a - \frac{1}{2}\right)^2 - \frac{3\varepsilon}{8}\right]^2$$

so that

$$a_{1,2} = \frac{1}{2} \mp \sqrt{\frac{3\varepsilon}{8}} \quad \text{and} \quad \Lambda = \frac{4}{3}\, kT.$$

Therefore

$$l_\tau = \frac{1}{2\sqrt{\varepsilon}} \sqrt{\frac{\kappa_{ij}\tau_i\tau_j}{kT}} \quad \text{and} \quad \gamma_\tau = \frac{\mathfrak{n}}{2}\, \varepsilon^{3/2} \sqrt{kT\kappa_{ij}\tau_i\tau_j},$$

the latter expressions quantify the dependence of macroscopic system characterisics on ε, that is, on non-ideality parameter *W*. Also power scaling laws can be derived at this point, in particular $\gamma \sim l_\tau^{-3}$ as $\varepsilon \to 0$.

DYNAMICS OF PHASE SEPARATION

In this section we describe typical numerical solutions of the basic equation (27). All solutions were obtained using the COMSOL Multiphysics implementation of the finite-elements method. The main goal is to illustrate important features of the phase decomposition process with special attention on specific effects resulting from the anisotropy of the interfacial energy.

To begin with we introduce suitable dimensionless variables for equation (27), because the specific values of κ_{ij} are unknown. Fortunately, to a large extent the actual results depend only on the dimensionless ratios of the main values κ_1, κ_2 and κ_3. To proceed, we introduce the normalized coordinates

$$\bar{x} = \frac{x}{l}, \quad \bar{y} = \frac{y}{l}, \quad \bar{z} = \frac{z}{l},$$

where the characteristic length scale l will be specified later. The corresponding diffusion time scale is l^2/D and the normalized time reads

$$\bar{t} = \frac{Dt}{l^2}.$$

It is also natural to measure the energy per atom g in the kT units

$$\bar{g} = \frac{g}{kT}.$$

Altogether, the basic equation (27) takes the form

$$\bar{\partial}_t a = \bar{\nabla} \cdot \left[a(1-a)\bar{\nabla}\left(\frac{\partial \bar{g}}{\partial a} - \bar{\kappa}_{ij}\bar{\partial}_i\bar{\partial}_j a\right)\right],$$

where $\bar{\partial}$ indicates derivative over dimensionless variables and

$$\bar{\kappa}_{ij} = \frac{\kappa_{ij}}{l^2 kT}.$$

In the isotropic case one can choose l in such a way that $\bar{\kappa}_{ij}$ reduces to a unit tensor so that

$$\bar{\partial}_t a = \bar{\nabla} \cdot \left[a(1-a)\bar{\nabla}\left(\frac{\partial \bar{g}}{\partial a} - \bar{\nabla}^2 a\right)\right].$$

Specific models only differ in the expression for $\bar{g}(a)$. The contribution of the interfacial energy is described in a universal manner for all isotropic systems. In particular, for the regular solution model (eq. 21) it is evident that only the free energy of mixing is important and one can safely assume that

$$\bar{g} = a \ln a + (1-a)\ln(1-a) + \chi a(1-a),$$

where the only dimensionless parameter

$$\chi = \frac{W}{kT}$$

is left. In the anisotropic case one can make a rotation to the main axes and then choose $\bar{\kappa}_2 = 1$ so that

$$\bar{\kappa}_{ij} = \mathrm{diag}\left(\frac{\kappa_1}{\kappa_2}, 1, \frac{\kappa_3}{\kappa_2}\right).$$

In particular, the interface effect on a two-dimensional system is actually determined by a single dimensionless parameter

$$\eta = \frac{\kappa_1}{\kappa_2}.$$

For the regular solution model (eq. 21) the dynamics in two spatial dimensions is determined by the equation

$$\bar{\partial}_t a = \bar{\nabla} \cdot \{[1 - 2\chi a(1-a)]\bar{\nabla} a - a(1-a)\bar{\nabla}(\eta\bar{\partial}_x^2 a + \bar{\partial}_y^2 a)\}. \qquad (43)$$

Equation (43) contains only two parameters χ and η. Corresponding solutions for $a(\bar{x}, \bar{y}, \bar{t})$ are discussed in the remainder of this section. To return to physical units for space and time the system specific values of l and D/l^2 should be given. Their choice is discussed in the accompanying paper (see also Takei and Shimizu, 2003; Shimizu and Takei, 2005a, 2005b).

Snapshots of the three typical numerical solutions to the isotropic equation (43) taken at the same time for three different values of the initial concentrations are shown in figure 3. The initial concentration $a(\bar{x}, \bar{y}, 0)$ is set to be space-uniform with a small additional random perturbation, the uniform value a_0 is chosen between the spinodal values (see three black dots in fig. 2). The symmetrical initial value $a_0 = 0.5$ corresponds to the equal production of both phases with pronounced interfingered, co-continuous morphology. For smaller or larger values of a_0 one phase dominates over the other and the typical host-precipitate microstructure is obtained. After the

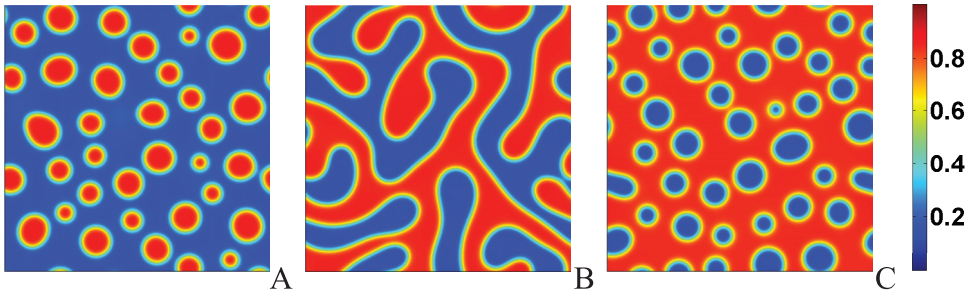

Fig. 3. Examples of 2D numerical solutions to the isotropic equation (43) for $\chi = 2.5$ and $\eta = 1$. Integration region is $50l \times 50l$, periodic boundary conditions are applied. The initial concentration $a(\bar{x}, \bar{y}, 0)$ takes a uniform value a_0 with some additive noise. Density plot of $a(\bar{x}, \bar{y}, \bar{t})$ for $\bar{t} = 2000$ is shown for three values of a_0. (A) $a_0 = 0.35$, particulate morphology for the second phase. (B) $a_0 = 0.5$, labyrinth-like co-continuous morphology. (C) $a_0 = 0.65$, particulate morphology for the first phase.

initial phase separation the system is in the coarsening stage, which is of interest for many applications (Toral and others, 1995). Let us now investigate how the anisotropy $\eta \neq 1$ affects the coarsening.

To this end we produced numerical solutions of equation (43) for different values of χ and η starting from the uniform system state with some additional noise. Then we compared the corresponding time series for the same value of $\chi > 2$ and several values of η. Figure 4 shows six consecutive snapshots of the isotropic $\eta = 1$ case in the regime of Ostwald ripening (see, for example Ratke and Voorhees, 2002). After a short initial stage of free growth the particles start to interact with each other and the larger

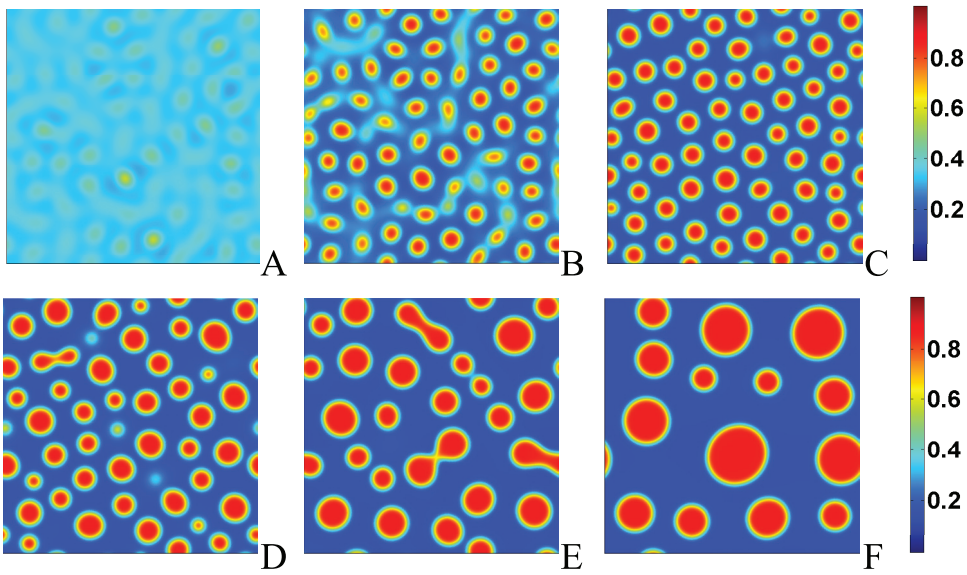

Fig. 4. 2D numerical solution to the equation (43) for $\chi = 2.5$, $\eta = 1$, and $a_0 = 0.35$. Integration region and boundary conditions as in figure 3. A time series for $a(\bar{x}, \bar{y}, \bar{t})$ is shown. (A): $\bar{t} = 100$ initial stage of instability; (B) and (C): $\bar{t} = 200$ and $\bar{t} = 450$, respectively. The particles grow freely, their number does not change much. (D) and (E): $\bar{t} = 1430$ and $\bar{t} = 2950$, respectively. Coarsening stage of the particle growth: the number of particles permanently decreases. Some particles grow at the expense of the others. (F): $\bar{t} = 10000$. Several larger particles are left, their further evolution is exceedingly slow. All particles are in a quasi-equilibrium state and look like perfect circles.

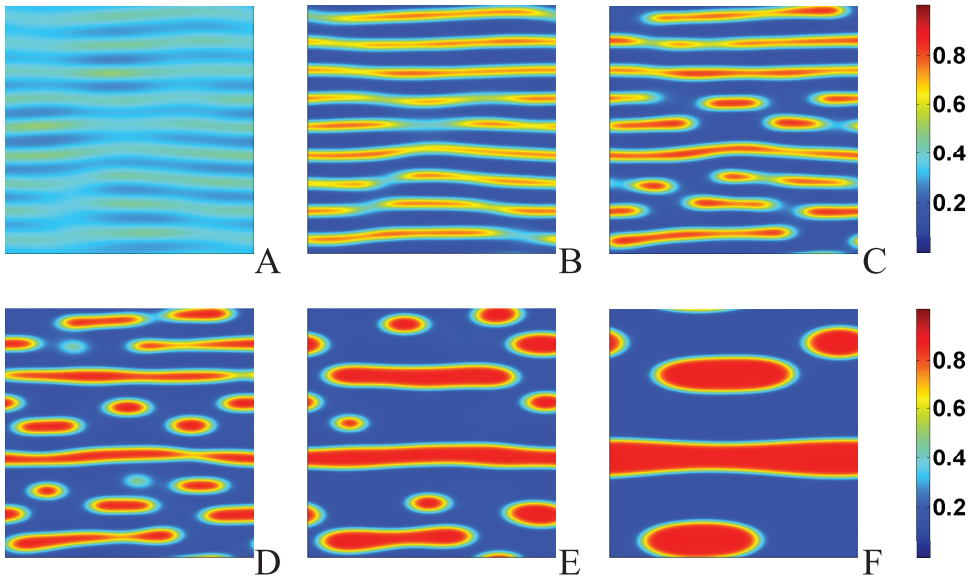

Fig. 5. 2D numerical solution to the anisotropic equation (43) for $\chi = 2.5$, $\eta = 5$. The initial conditions and integration region as in figure 4. (A): $\bar{t} = 250$; (B): $\bar{t} = 400$; (C): $\bar{t} = 600$; (D): $\bar{t} = 880$; (E) $\bar{t} = 1900$; (F): $\bar{t} = 10000$. During the initial separation stage a lamellar microstructure develops, which is successively lost during the coarsening stage. All particles have a pronouncedly elongated shape owing to the intrinsic anisotropy of the system.

particles grow on the expense of the smaller ones. Note, that isolated particles have an approximately round shape, as prescribed by the symmetry of the system. Finally only several weakly interacting large particles are left, their evolution is now extremely slow. Figure 5 shows the instability dynamics for the anisotropic $\eta = 5$ case. The main stages of the instability development are similar to the isotropic case, however, the particles have a clearly elongated shape. The interfaces are characterized by a normal vector $\boldsymbol{\tau}$, their contribution to the system free energy is proportional to $\kappa_{ij}\tau_i\tau_j$ accord with equation (42). Therefore the most preferred orientation is such that $\kappa_{ij}\tau_i\tau_j$ is minimized, for instance, the particles are elongated along the *OX* axis in figure 5. One also sees that the interface width of particles in figure 5 depends on orientation as predicted by equation (41).

Another interesting effect is that for finite systems with uneven dimensions the critical system size (eq. 32), at which the system becomes unstable with respect to spinodal decomposition, depends on direction. In particular, a two-dimensional system, which has considerably different spatial dimensions, may be stable in one direction and unstable in the other. In this case stripes are formed parallel to the short dimension of the system, even if the interfacial energy is isotropic (fig. 6). This may be relevant in the context of phase separation in thin films and for cellular precipitation. For the anisotropic case an artificially narrow domain is not required for the formation of stripes, as illustrated in figure 7.

CONCLUSIONS

In conclusion let us summarize our findings. The original analysis of spinodal decomposition by Cahn and Hilliard was adopted for counterdiffusion in an *isotropic* system. To this end the system free energy $g(a)$ was modified by inclusion of the gradient term

$$g(a) \rightarrow g(a) + \frac{1}{2}\kappa(\nabla a)^2,$$

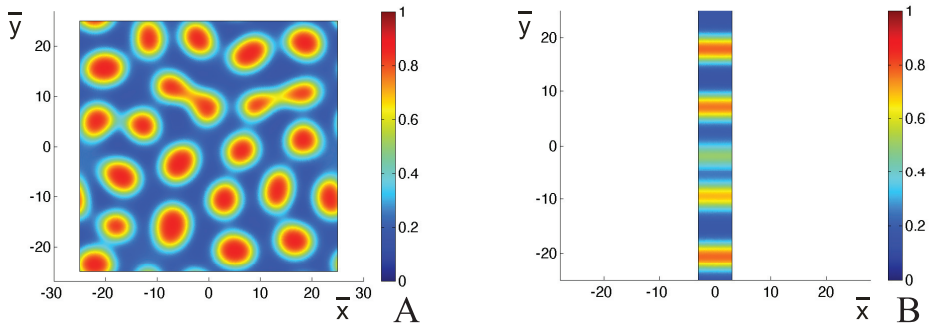

Fig. 6. 2D numerical solutions of the isotropic equation (43) for or $\chi = 2.5$, $\eta = 1$, and $a_0 = 0.35$. The effect of different system dimensions is illustrated by solutions at $\bar{t} = 180$. (A) The integration region is $50l \times 50l$, an isotropic decomposition is observed. (B) The integration region is $6l \times 50l$. The system is stable in x direction and evolves to a stripes pattern due to separation in y direction.

where the free energy per atom g is given as a function of composition a and, if necessary, other system parameters such as pressure and temperature.

This extension of the free energy model was originally suggested by van der Waals (van der Waals, 1893). In the context of the spinodal decomposition problem it was shown that an arbitrary dependence of the free energy on spatial derivatives of a can be reduced to the above one as long as Taylor expansion in terms of ∇a is allowed. In particular, contribution of interfacial energy is described by a new parameter κ, that is, any equilibrium system property can be expressed in terms of a suitable set of thermodynamics variables and κ. An intrinsic isotropy of the system in question plays an important role here, among other things $(\nabla a)^2$ and $\nabla^2 a$ are the only combinations of the second derivatives that are invariant under rotations and the contribution of the second combination can be eliminated by means of the divergence theorem.

In many important situations the underlying systems are *anisotropic* and corresponding generalization of the decomposition model is required. Cahn (1962) has considered elastic anisotropy by allowing for a small change in the total concentration of atoms and thereafter accounting for the induced stresses under the condition that phase boundaries remain coherent. Anisotropic diffusion was considered in Lefever and Carati (1995). In this contribution we investigate another principle possibility, namely a possible anisotropy in the interfacial energy itself. The total atomic concentra-

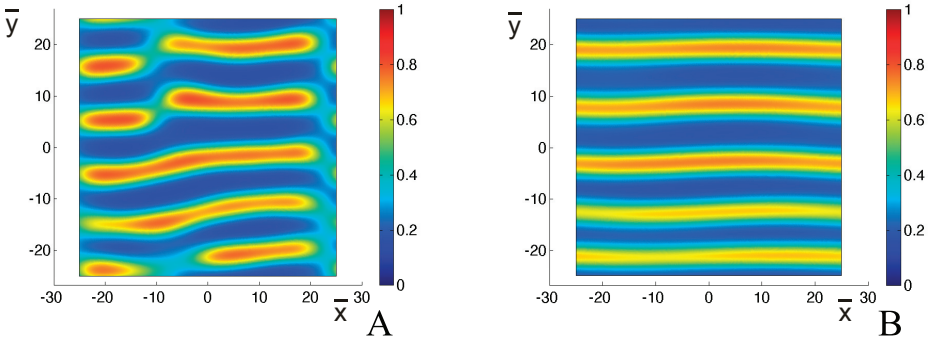

Fig. 7. The same as in figure 6, but for $\eta \gg 1$. Now, a narrow domain is not necessary for stripes formation. (A): $\eta = 5$, (B): $\eta = 7$. Both solutions are given for $\bar{t} = 180$.

tion as well as system temperature and pressure remain uniform. However lamellae have an elongated equilibrium shape that minimizes the system free energy.

The corresponding model for the system free energy per atom reads

$$g(a) \rightarrow g(a) + \frac{1}{2} \sum_{i,j=1,2,3} \kappa_{ij} \partial_i a \partial_j a,$$

and is characterized by a second order tensor κ_{ij}, the latter is symmetric and positively defined. Furthermore, following the original strategy of Cahn and Hilliard it is possible to demonstrate that after a proper transformation the above equation is applied to any crystal structures, which possesses mirror symmetry. In particular, in two (three) spatial dimensions the system is described by one (two) additional parameters, namely dimensionless ratios of the principal values of κ_{ij}. After doing so we obtain an anisotropic generalization of the Cahn-Hilliard equation and investigate its properties. For instance, if orientation of the interface is locally characterized by a normal vector $\boldsymbol{\tau}$, the interfacial energy is proportional to $\sqrt{\kappa_{ij}\tau_i\tau_j}$. Another interesting effect is that the critical (minimum) system size, at which decomposition can occur, is now anisotropic. In particular the system can be unstable in one direction and stable in the others. Here the spinodal decomposition leads to the growth of a lamellar pattern. Finally we investigated phase decomposition in the anisotropic system numerically. Here, the decomposition products have a pronounced shape anisotropy.

ACKNOWLEDGMENTS

This work was funded by the Deutsche Forschungsgemeinschaft, project AB 314/3-1 as part of FOR 741. We are indebted to I. Shimizu, who provided detailed comments on the manuscript, and we gratefully acknowledge the critical remarks made by D. Schmid.

References

Abinandanan, T. A., and Haider, F., 2001, An extended Cahn-Hilliard model for interfaces with cubic anisotropy: Philosophical Magazine, v. 81, n. 10, p. 2457–2479, doi: 10.1080/01418610108217158.

Bettinson, B., and Rowlands, R., 1996, Stability of the one-dimensional kink solution to a general Cahn-Hilliard equation: Physics Review E, v. 54, n. 6, p. 6102–6108, doi:10.1103/PhysRevE.54.6102.

Brizi, E., and Mellini, M., 1992, Kinetical modelling of exsolution textures in igneous pyroxenes: Acta Vulcanologica, v. 2, p. 87–93.

Brown, W. L., and Parsons, I., 1984, Exsolution and coarsening mechanisms and kinetics in an ordered cryptoperthite series: Contributions to Mineralogy and Petrology, v. 86, p. 3–18, doi:10.1007/BF00373706.

——— 1988, Zoned ternary feldspars in the Klokken intrusion: exsolution microtextures and mechanisms: Contributions to Mineralogy and Petrology, v. 98, p. 444–454, doi:10.1007/BF00372364.

Cahn, J. W., 1962, Coherent fluctuations and nucleation in isotropic solids: Acta Metallurgica, v. 10, p. 907–913.

——— 1968, Spinodal decomposition: Transactions of the Metallurgical Society of AIME, v. 242, n. 2, p. 166–180.

Cahn, J. W., and Hilliard, J. E., 1958, Free Energy of a Nonuniform System. I. Interfacial Free Energy: The Journal of Chemical Physics, v. 28, n. 2, p. 258–267, doi:10.1063/1.1744102.

Cahn, J. W., and Novick-Cohen, A., 1994, Evolution equations for phase separation and ordering in binary alloys: Journal of Statistical Physics, v. 76, n. 3–4, p. 877–909.

Cheng, Z., Sakamoto, T., Takahashi, M., Kuramoto, Y., Owari, M., and Nihei, Y., 1998, Development of ion and electron dual focused beam apparatus for high spatial resolution three-dimensional microanalysis of solid materials: Journal of Vacuum Science and Technology, B, Microelectronics and Nanometer Structures, v. 16, p. 2473–2478.

COMSOL multiphysics: http://www.femlab.com/.

Fischer, F. D., Berveiller, M., Tanaka, K., and Oberaigner, E. R., 1994, Continuum mechanical aspects of phase transformations in solids: Archive of Applied Mechanics, v. 64, n. 2, p. 54–85.

Golla-Schindler, U., O'Neill, H. S. C., and Putnis, A., 2005, Direct observation of spinodal decomposition in the magnetite-hercynite system by susceptibility measurement and transmission electron microscopy: The American Mineralogist, v. 90, p. 1278–1283, doi:10.2138/am.2005.1849.

Grove, T., 1982, Use of exsolution lamellae in lunar clinopyroxenes as cooling rate speedometers—an experimental calibration: The American Mineralogist, v. 67, p. 251–268.

Heermann, D., 1984, Test of the Validity of the Classical Theory of Spinodal Decomposition: Physical Review Letters, v. 52, n. 13, p. 1126–1128, doi:10.1103/PhysRevLett.52.1126.
Hovis, G. L., Kroll, H., Breit, U., and Yund, R. A., 2003, Elastic strain enthalpies of exsolution: HF solution calorimetric experiments on alkali aluminosilicate and aluminogermanate feldspars: The American Mineralogist, v. 88, p. 547–555.
Kral, M. V., Mangan, M. A., Spanos, G., and Rosenberg, R. O., 2000, Three-dimensional analysis of microstructures: Materials Characterization, v. 45, p. 17–23, doi:10.1016/S1044-5803(00)00046-2.
Kuhl, E., and Schmid, D. W., 2007, Computational modeling of mineral unmixing and growth: Computational Mechanics, v. 39, n. 4, p. 439–451, doi:10.1007/s00466-006-0041-1.
Lefever, R., and Carati, D., 1995, Intrinsic patterns in anisotropic multicomponent diffusive systems at equilibrium: Physica A, v. 213, p. 90–104, doi:10.1016/0378-4371(94)00150-R.
McCallister, R. H., and Yund, R. A., 1977, Coherent exsolution in Fe-free pyroxenes: The American Mineralogist, v. 62, p. 721–726.
Nauman, E. B., and He, D. Q., 2001, Nonlinear diffusion and phase separation: Chemical Engineering Science, v. 56, n. 6, p. 1999–2018, doi:10.1016/S0009-2509(01)00005-7.
Onsager, L., 1931, Reciprocal relations in irreversible processes. I: Physical Review, v. 37, n. 4, p. 405–426.
Price, G. D., 1982, Exsolution microstructures in titanomagnetites and their magnetic significance: Physics of the Earth and Planetary Interiors, v. 23, p. 2–12, doi:10.1016/0031-9201(80)90078-3.
Ratke, L., and Voorhees, P. W., 2002, Growth and coarsening: Ostwald ripening in material processing: Berlin, Springer, 295 p.
Shewmon, P. G., 1963, Diffusion in Solids: New York, McGraw-Hill, 203 p.
Shimizu, I., and Takei, Y., 2005a, Temperature and compositional dependence of solid-liquid interfacial energy: Application of the Cahn-Hilliard theory: Physica B: Condensed Matter, v. 362, p. 169–179, doi:10.1016/j.physb.2005.02.008.
——— 2005b, Thermodynamics of interfacial energy in binary metallic systems: Influence of adsorption on dihedral angles: Acta Materialia, v. 53, p. 811–821, doi:10.1016/j.actamat.2004.10.033.
Shinozaki, A., and Oono, Y., 1993, Dispersion relation about the kink solution of the Cahn-Hilliard equation: Physical Review E, v. 47, n. 2, p. 804–811, doi:10.1103/PhysRevE.47.804.
Smith, J. V., and Brown, W. L., 1988, Feldspar Minerals, v. 1: Crystal Structures, Physical, Chemical, and Microtextural Properties: Berlin, Springer Verlag, 828 p.
Takei, Y., and Shimizu, I., 2003, The effects of liquid composition, temperature, and pressure on the equilibrium dihedral angles of binary solid-liquid systems inferred from a lattice-like model: Physics of the Earth and Planetary Interiors, v. 139, p. 225–232, doi:10.1016/j.pepi.2003.08.004.
Taylor, J. E., and Cahn, J. W., 1998, Diffuse interfaces with sharp comers and facets: Phase field models with strongly anisotropic surfaces: Physica D, v. 112, n. 3–4, p. 381–411, doi:10.1016/S0167-2789(97)00177-2.
Toral, R., Chakrabarti, A., and Gunton, J. D., 1995, Large scale simulations of the two-dimensional Cahn-Hilliard model: Physica A, v. 213, n. 1–2, p. 41–49, doi:10.1016/0378-4371(94)00146-K.
van der Waals, J. D., 1893, The Thermodynamic Theory of Capillarity Under the Hypothesis of a Continuous Variation of Density, originally published in Dutch: Verhandel. Konink. Akad. Weten., Amsterdam, v. 1, n. 8, 56 p., translation by Rowlinson, J. S., 1979: Journal of Statistical Physics, v. 20, p. 200–244, doi:10.1007/BF01011514.
Watanabe, S., Kitamura, M., and Morimoto, N., 1985, A transmission electron microscope study of pyroxene chondrules in equilibrated L-group chondrites: Earth and Planetary Science Letters, v. 72, p. 87–98, doi:10.1016/0012-821X(85)90119-0.
Weinbruch, S., and Muller, W. F., 1995, Constraints on the cooling rates of chondrules from the microstructure of clinopyroxene and plagioclase: Geochimica et Cosmochimica Acta, v. 59, n. 15, p. 3221–3230, doi:10.1016/0016-7037(95)00210-Q.
Weinbruch, S., Muller, W. F., and Hewins, R. H., 2001, A transmission electron microscope study of exsolution and coarsening in iron-bearing clinopyroxene from synthetic analogues of chondrules: Meteoritics and Planetary Science, v. 36, p. 1237–1248.
Weinbruch, S., Styrsa, V., and Muller, W. F., 2003, Exsolution and coarsening in iron-free clinopyroxene during isothermal annealing: Geochimica et Cosmochimica Acta, v, 67, p. 5071–5082, doi:10.1016/S0016-7037(03)00205-9.
Wise, S., Kim, J., and Lowengrub, J., 2007, Solving the regularized, strongly anisotropic Cahn-Hilliard equation by an adaptive nonlinear multigrid method: Journal of Computational Physics, v. 226, n. 1, p. 414–446, doi:10.1016/j.jcp.2007.04.020.
Yund, R. A., and Chapple, W., 1980, Thermal histories of two lava flows estimated from cryptoperthite lamellar spacings: The American Mineralogist, v. 65, p. 438–443.
Yund, R. A., and Davidson, P., 1978, Kinetics of lamellar coarsening in cryptoperthites: The American Mineralogist, v. 63, p. 470–477.
Yund, R. A., McLaren, A. C., and Hobbs, B. E., 1974, Coarsening kinetics of exsolution microstructure in alkali feldspar: Contributions to Mineralology and Petrology, v. 48, p. 45–55.